A SIMULATION STUDY ON EFFECT OF NOZZLE GEOMETRY ON FLAMELESS COMBUSTION OF NON-PREHEATED METHANE GAS

by

Yazhu Zhang[a], Congxi Liu[a], Zhuben Huang[b], Jun Huang[a,c,*], Li Zhang[d], Kai Li[a]

a School of Energy and Environment, Inner Mongolia University of Science and Technology, Baotou 014010, China;

b China National Air Separation Engineering Co.Ltd, Hangzhou 310000, China;

c Collaborative Innovation Center of Integrated Exploitation of Bayan-Obo Multi-Metal Resources, Inner Mongolia University of Science and Technology, Baotou 014010, China;

d School of Energy and Power Engineering, University of Shanghai for Science and Technology, Shanghai 200093, China

In this paper, the effects of different burner configurations on the characteristics of flameless combustion were evaluated by comparing the temperature field, NO_x, OH and H_2CO at different burner inlet velocity and angles through a combination of experimental and numerical simulations. The results show that increasing the burner inlet angle and gas velocity is imperative in achieving the flameless combustion, increasing the recirculation rate in the furnace, making the temperature distribution in the furnace uniform, and reducing the emission of NO_x at the end of the furnace. During the simulation of flameless combustion, it was found that OH radicals and H_2CO radicals were well correlated with the reaction exothermic zone, and the Reynolds number was positively correlated with the recirculation rate in the furnace. With the increase of Reynolds number, the entrainment rate of flue gas increases, and the combustion state is closer to flameless combustion. When recirculation rate $Kv > 2$, combustion becomes flameless. Through the summary analysis of the data, it can be found that there is a critical Reynolds number for the burner to achieve flameless combustion, and flameless combustion occurs only when the Reynolds number is greater than 1.0×10^4.

Key words: *Flameless combustion, methane combustion, Numerical simulation, NO_x emission, Temperature distribution*

1. Introduction

With the continuous advances in combustion technology, the industry requirements to improve the combustion efficiency of industrial furnaces become more stringent [1] especially the requirements to meet the ultra-low pollution emission standards [2-4]. The combustion technologies currently used include oxy-fuel combustion technology [5], air staging combustion technology [6], fuel staging combustion technology [7], and flue gas recirculation technology [8]. In the pursuit of higher combustion efficiency and lower pollutant emissions, researchers are constantly searching for new combustion technologies, and flameless combustion is one of the important areas. With the continuous research on combustion technology, researchers found that flameless combustion technology has such advantages as uniform heat flow distribution, high combustion efficiency, and low pollutant emission advantages [2,9-15]. The advantages of the flameless combustion are: there is no obvious flame front during fuel combustion; the temperature distribution in the furnace is uniform with the peak temperature not higher than 1 400 K; the CO and NO_x emissions in the flue gas are not higher than 20 mg/m^3.

Katsuki conducted a study on industrial furnace combustion and concluded that low oxygen concentration combustion, achieved through diluting oxygen in the furnace flue gas, can be an effective method for reducing NO_x emissions by means of flameless combustion [16]. Researchers at the University of Adelaide [17-19] investigated the effects of different chemical reaction mechanisms on preheating flameless combustion. By combining experimental and simulation data, they found that the flameless combustion flame lift and the phenomenon of overall slow reaction should be considered during flameless combustion simulation. Results from Dally *et al* [20-22] showed that during flameless combustion, the combustion reaction zone gradually expands due to the increase in heat input, and the reaction zone moves from the burner outlet to the nozzle of the burner. Huang *et al* [23] found that the flameless natural gas combustion mode in industrial furnaces exhibited better combustion performance than the conventional swirl diffusion combustion mode. Currently, many burners can achieve flameless combustion technology, such as the flameless burner built by the University of Adelaide, Australia [24], the flameless burner built by Delft University of Technology, the Netherlands [25], the preheated air flameless burner built by Lisbon University of Technology [26], the flameless burner built by Poznan University of Technology [27], and the flameless burner built by the Linde Group [28]. However, in these studies, achieving flameless combustion requires preheating of the air.

In the current literature, there are few studies on achieving flameless combustion under normal temperature air conditions and fewer applications of the GRI-Mech 3.0 detailed chemical reaction mechanism for flameless combustion of methane. In this research, the flameless combustion state was achieved experimentally with normal temperature air was achieved experimentally by increasing the incidence velocity of air and fuel, and the temperature distribution in the furnace under the flameless combustion state was measured experimentally. The detailed chemical reaction mechanism of GRI-Mech 3.0 is used for numerical simulation to study the effects of different burner inlet angles and gas velocity on the temperature field of flameless combustion of normal temperature air, NO_x, OH and H_2CO.

2. Experimental equipment and numerical simulation

A schematic of the combustor used in this study is shown in fig. 1. The experiments were conducted using a symmetrical jet nozzle structure, four 4 mm equidistant nozzles in a 40 mm circle, and a nozzle angle of 7°. The flameless combustion furnace has a length of 460 mm, an inner diameter of 150 mm, and an outer diameter of 180 mm. The inside of the furnace is a 5 mm thick steel pipe and the furnace is surrounded by a 10 mm thick glass fiber blanket, which is used to provide the insulation of the furnace and keep the furnace flue gas temperature above the auto-ignition point of the fuel. Experiments were performed with methane as fuel and air as the oxidizer, both at 298 K, where the methane volume flow rate was 1 m^3/h and the air volume flow rate used for methane combustion was 10 m^3/h. In the experiment, flameless combustion without air preheating was realized based on the following two points: first, the furnace needs to be heated sufficiently so that the internal working temperature of the furnace is greater than the spontaneous combustion point of the combustible material; second, the flame burner used a nozzle with a smaller inlet aperture to enhance the jet at the exit of the nozzle so as to achieve the effect that the flame front is completely blown away by the exit jet.

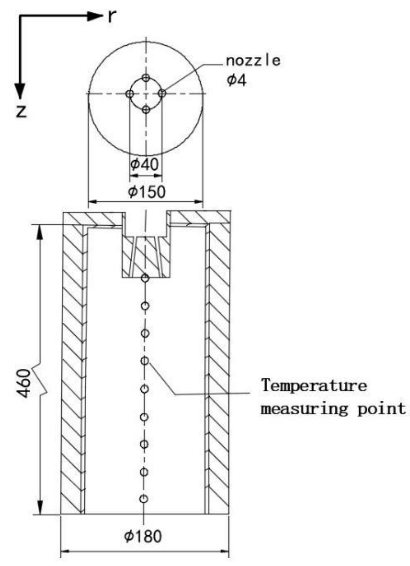

Fig. 1. Schematic of the combustor

In the fig. 2, are shown the combustion images of methane transition from flaming combustion to flameless. The (a) state is the methane flaming combustion state, and the flame front is more obvious in this state. With the continuous increase of the inlet air flow volume, the jet flow volume is increasing, and the flame rigidity is weakening, when the air volume is increased to 6 m^3/h, the flame is gradually transformed to a flameless combustion state, from the (a) state to the (b) state, (b) state is in the methane flaming combustion to flameless combustion transition state, the root of the flame light blue flame is intermittent; when the air volume is increased to 9 m^3/h, the combustion state is transformed to (c) state. From the fig. 2, it can be deduced that there is no obvious flame front in the furnace in the flameless combustion state. After the combustion changed to the flameless combustion state, temperature measurements were performed in the experiment using multiple type S platinum-rhodium thermocouples. These measurement points were arranged along the center axis of the furnace, with one temperature measurement point set every 50 mm. When the temperature change was less than 1.5 K per minute, temperature acquisition was performed, and the acquisition process lasted at least 180 seconds, and the mean temperature of that period was used as the value. The measured temperatures at the thermocouples were corrected to accommodate the radiation losses.

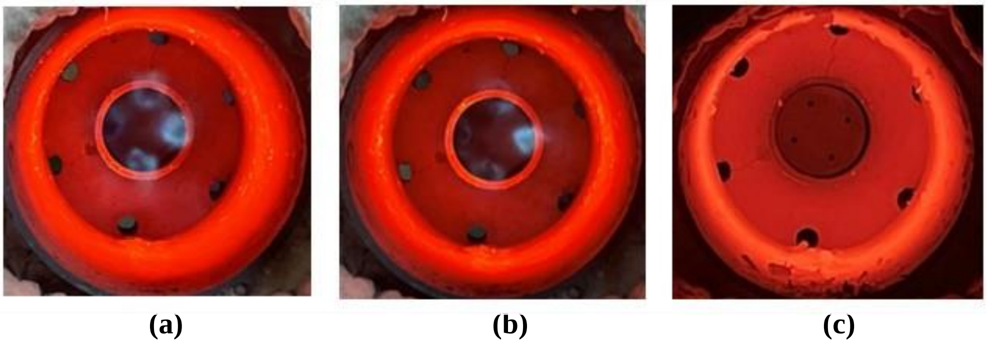

(a) **(b)** **(c)**

Fig. 2. Images of flaming to flameless combustion processes

Numerical simulations were performed using FLUENT software for steady-state calculations, and based on previous studies of flameless combustion numerical simulations [29], a modified standard k-ε equation model was used with the dissipation rate equation set to 1.6 [30]. The EDC model was used in conjunction with the detailed chemical reaction kinetics GRI-Mech 3.0 mechanism, and the Discrete Ordinate model was chosen for the radiative heat transfer model of the flameless combustion simulation and used in the weighted sum of the gray gas model. The SIMPLE algorithm was used for calculation and solution, and the second order upwind format was used for discrete format. The convergence was estimated on the basis that the residuals of the energy and radiation terms were less than 10^{-6} and the residuals of the other terms were less than 10^{-3}. Temperature distribution and inlet and outlet flow rates remain constant when convergence is reached. The computational grid was divided as shown in fig. 3, based on the symmetric design of the combustion chamber and the symmetric characteristics of the flow. A 1/4 combustion chamber model was established and the complete furnace computational domain was obtained by setting the symmetric boundary. The simulation boundary conditions were set as velocity inlet, pressure outlet, and constant wall temperature. The room temperature inlet air velocity is 8 m/s and the room temperature fuel inlet velocity is 89 m/s. The wall temperature was measured experimentally, and based on that the constant wall temperature was set to 1 123 K for methane. Changes in intake velocity and angle result in changes in recirculation rate. Recirculation rate Kv can be measured through:

$$Kv = \frac{M_e}{M_a + M_f} \tag{1}$$

Kv=0 if no recirculation and Kv=1 if Me = (Ma+Mf). where M_a and M_f denote mass flow rate of inlet air and fuel, respectively and Me is the mass flow rate of recirculated exhaust gas. Me is obtained:

$$Me = \iint_{\mathrm{Az}} \rho \mathrm{V}z dxdy \tag{2}$$

Kv=0 if no recirculation and Kv=1 if $Me = (Ma+Mf)$

where ρ is the mixture density and Az means the area with negative axial velocity (Vz < 0).

Re is obtained:

$$\mathrm{Re} = \frac{\rho u L}{\mu} \tag{3}$$

where ρ is the mixture density, u is the flow rate, L is the characterization length, and μ is the kinetic viscosity.

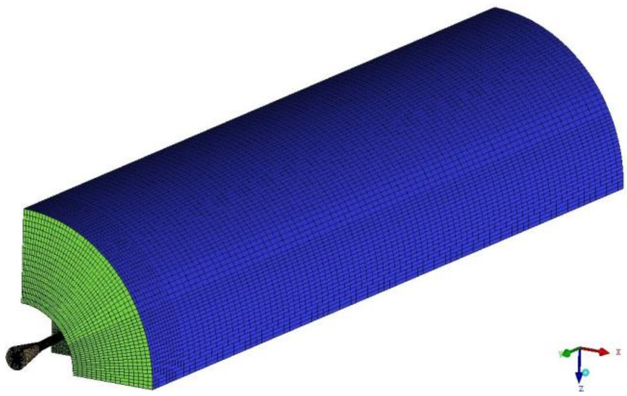

Fig. 3. Grid division diagram of flameless combustion experimental furnace

3. Results and discussion

This section presents the results and discussion of our study, which explored the effects of different burner configurations on the formation of flameless combustion by varying the inlet angle and inlet diameter of the burner. In order to achieve this objective, we evaluated 11 different configurations and compared the numerical simulation results with existing experimental data. The comparison showed good agreement between the two sets of data. The simulated working conditions are presented in tab. 1, while the results are illustrated in figs. 4 to 13.

Tab. 1. Simulation conditions

Working conditions	Inlet diameter (mm)	Incidence angle (°)
1	4	7
2	8	7
3	12	7
4	13	7
5	14	7
6	16	7
7	4	0
8	4	3
9	4	5
10	4	11
11	4	15

As shown in fig. 4, compares the simulated temperature measurement points against those of the experimental temperature measurement points with respect to different grid numbers. Computational grids of various densities (150 000 coarse grids, 460 000 medium grids, and 680 000 fine grids) were generated by utilizing ICEM to create a hexahedral mesh with various degrees of densification at the outlet and inlet. As shown in fig. 4, it can also be deduced that the temperature distribution trends of different grids are similar, indicating that the simulation results are not too sensitive to the three different grid densities set. Before the axial distance of 180 mm, the simulation results are about 50 K higher than the experimental results; between the axial distance of 180 mm and 330 mm, the simulation results are very close to the experimental results; after the axial distance of 330 mm, the outlet temperature drops sharply due to the influence of cold air return at the outlet, which leads to the deviation of the simulation results from the experimental results, but the overall change trend is similar. The number of 460 000 grids in the simulation process can meet the requirements of the numerical simulation of the combustor, and 460 000 grids are used in the subsequent numerical simulation of this study.

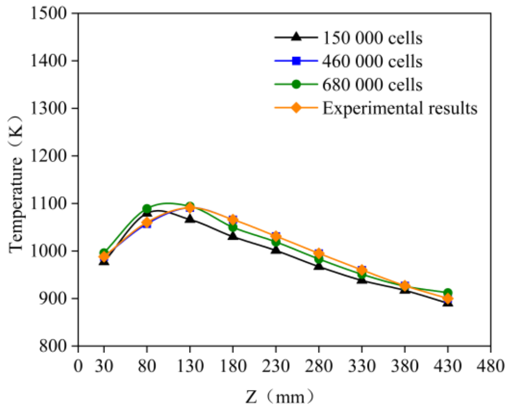

Fig. 4. Axial distribution of average gas temperature with different grid numbers

At constant flow rate, the inlet velocity of the burner increases as the burner inlet diameter becomes smaller. The effect of inlet velocity on the flameless combustion characteristics is investigated in the simulation by varying the inlet diameter. As shown in fig. 5, the axial distribution of the average temperature of the gas with different inlet diameters. It can be seen that as the inlet diameter decreases, the high-temperature zone moves forward, the peak temperature drops from 1 538 K to 1 215 K, the peak position moves back from 330 mm to 130 mm, and the temperature gradually becomes average. When the combustion is in the flameless combustion state, the temperature fluctuation is less than 15%, and the maximum temperature is less than 1 400 K.

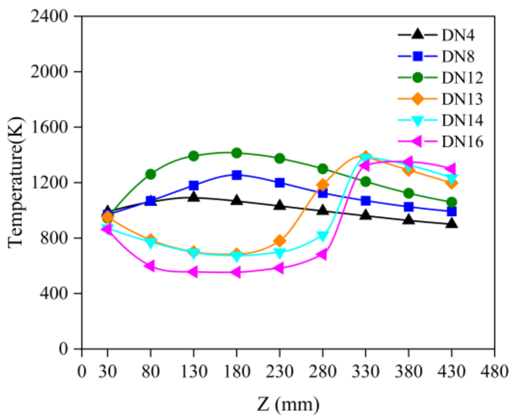

Fig. 5. Axial distribution of average gas temperature with different inlet

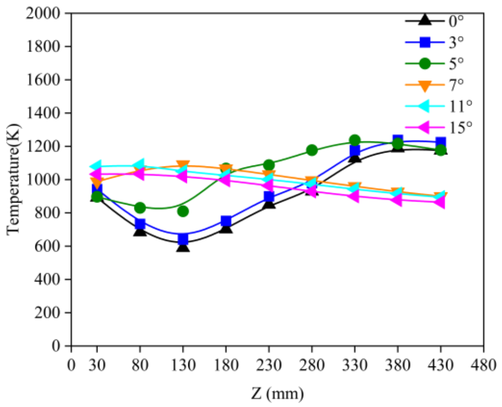

Fig. 6. Axial distribution of the average gas temperature at different inlet angles

The axial distribution of the average gas temperature at different inlet angles is shown in fig. 6. From the fig.6, it can be seen that the peak temperature in the furnace continuously decreases from about 1 200 K to about 1 000 K as the burner inlet angle increases.

Fig. 7 shows the variation of NO_x content in the furnace flue gas at the furnace exit for different burner inlet diameters. It was found that an inflection point in NO_x content occurs when the inlet diameter is 12 mm. When the diameter is larger than 12 mm, the high temperature zone is close to the outlet, resulting in the front-end temperature being lower than 1 150 K and the average temperature in the furnace chamber is low. As the diameter decreases, the average temperature in the chamber starts to increase and the NO_x emissions are mainly influenced by the thermal NO mechanism, leading to an increase in NO_x emissions. At this point, the process is mainly in a conventional flame combustion state. When the diameter is less than 12 mm, the reaction changes from the traditional flamed combustion state to a flameless combustion state, the average temperature in the furnace begins to decrease, and NO_x emissions begin to decline.

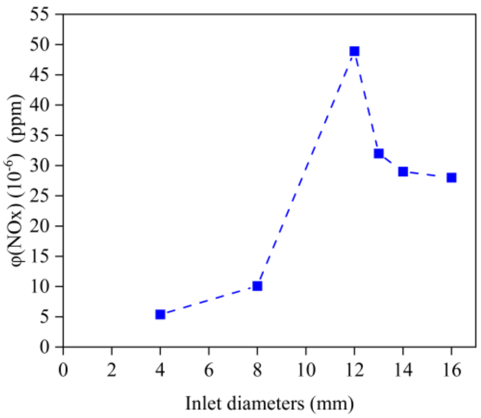

Fig. 7. NO_x emissions from the tail pollutants of the furnace with different inlet diameters

As shown in fig. 8, with the angle increase, the main combustion zone moves forward, the peak value keeps decreasing, the overall temperature distribution gradually tends to average, and the NO_x content in the furnace tail pollutant keeps decreasing. When the inlet angle is set to 0°, the high-temperature zone is close to the exit position, which is not conducive to the stability of flameless combustion. It was also found that when the overall temperature in the furnace was greater than 1 150 K, the NO_x generation increased with the increase of temperature.

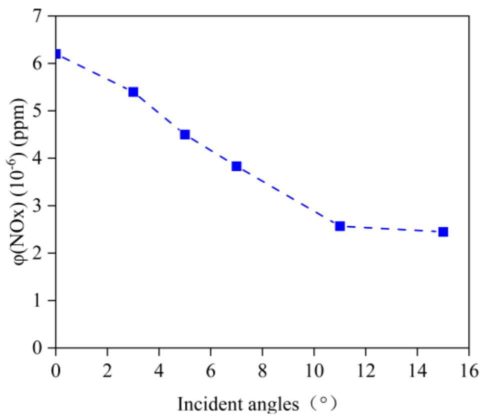

Fig. 8. NO_x emissions from furnace tail pollutants at different incident angles

In fig. 9 is shown the temperature field distribution contour plot for different burner inlet diameters, and the inlet diameters are 4 mm, 8 mm, 12 mm, 13 mm, 14 mm, and 16 mm from left to right. It was found that as the burner inlet diameter decreases, the flow of mixed fuel injection gradually increases and the mixing of reactants becomes more intense. It was also found that the flue gas dilution on the reactants steadily increased and that the temperature at each point in the furnace is higher than the fuel's self-ignition point, establishing flameless combustion. If the amount of flue gas dilution in the furnace is insufficient, that is, when the burner inlet diameter is greater than 12 mm, the combustion state in the furnace will change from flameless combustion to conventional flame combustion, which is characterized by a high peak temperature.

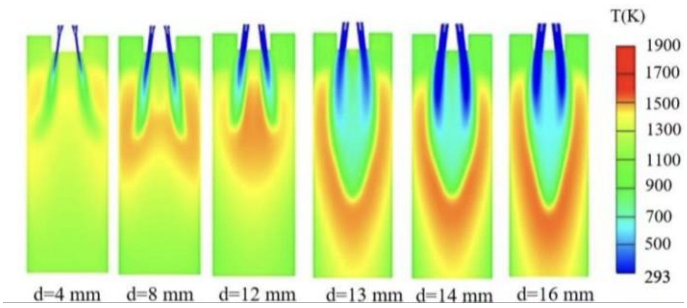

Fig. 9. Contour plots of temperature field distribution for different burner inlet diameters

In fig. 10 is shown the temperature distribution contour plot for different burner inlet angles, and the inlet angles are 0°, 3°, 5°, 7°, 11° and 15° from left to right, respectively. It was found that as the inlet angle increases, the high temperature zone gradually moves forward, the temperature distribution in the furnace gradually tends to be more uniform, and the flame is more dispersed. This flow field structure forms a small recirculation zone in the area near the burner. It was also found that as the angle increases, the recirculation zone moves toward the burner inlet, and the flue gas recirculation zone in the furnace is influenced by the angle of the burner inlet. Finally, the degree of fuel and air mixing in the flue gas recirculation zone increases with the increase of the burner inlet angle.

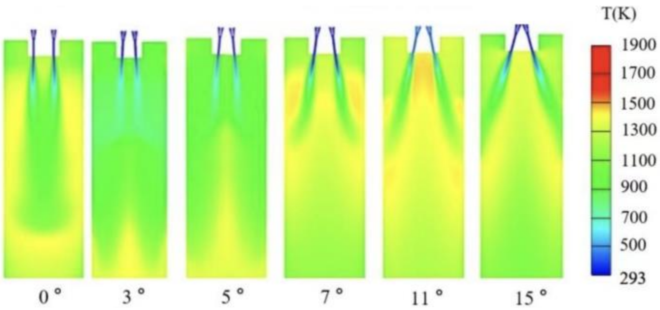

Fig. 10. The temperature distribution contour plot for different burner inlet angles

From the figs. 9, 10 and 11, it is clear that the temperature peak and OH peak positions overlap, and the temperature peak at which the reaction is the most intense can be considered to be the most intense and the heat is the largest, thus forming a local high temperature. Furthermore, as the diameter keeps decreasing from time to time with the increasing speed, the OH zone keeps decreasing and moving forward, and the combustion high temperature zone also keeps decreasing.

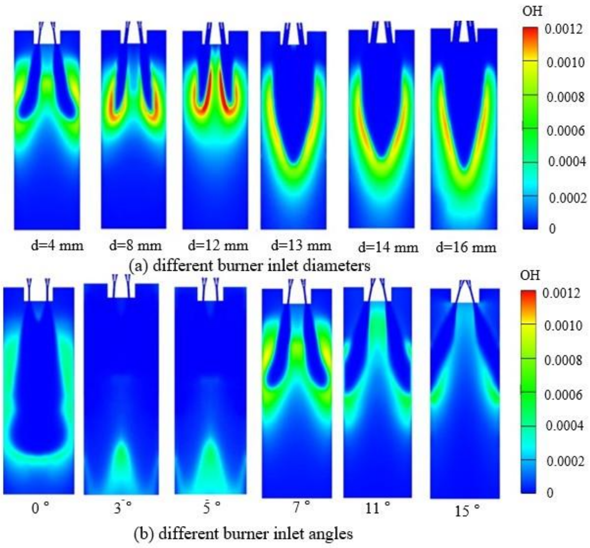

Fig. 11. OH distribution contour plot

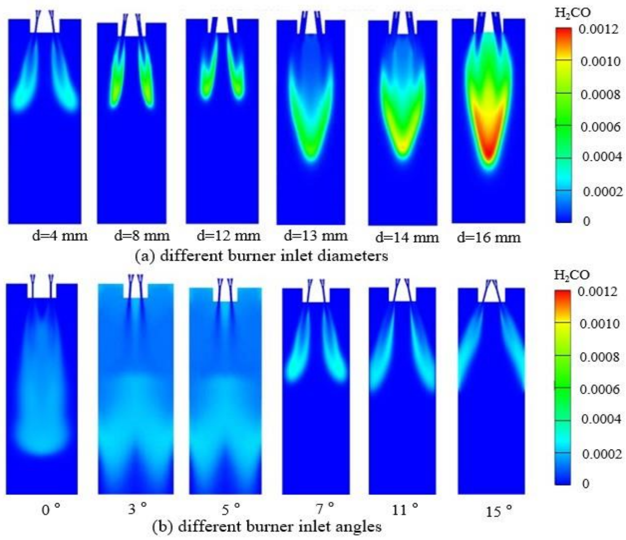

Fig. 12. H_2CO distribution contour plot for different burner inlet diameters

Comparing the figs. 9, 10 and 12 shows us that the correlation between temperature and the cloud diagram of H_2CO radical distribution, it was found that H_2CO radicals mainly appear in the low-temperature region of the reaction, and H_2CO radicals represent the intensity of the combustion reaction in the low-temperature region, which is an important intermediate product in the study of combustion. Also, it was deduced that the concentration of H_2CO radicals decreases sharply, which means that H_2CO radicals are not the main intermediate component in the high temperature region, that is to say, in the high-temperature region, H_2CO radicals would be rapidly consumed to produce the subsequent products of the oxidation reaction.

In this study, the Reynolds number was used as a dimensionless parameter to control the occurrence of flameless combustion while the recirculation rate *Kv* was used to measure the dilution of the reactants in the flue gas. The relationship between the Reynolds number and the recirculation rate at the nozzle was shown in fig. 13. Combining experimental and simulation data, the researchers found that the Reynolds number increased as the inlet diameter decreased, and the amount of flue gas circulation in the furnace increased as the Reynolds number continues to increase. Flameless combustion occurs when *Kv* > 2. The relationship between the Reynolds number and flue gas circulation was almost linear, with an increase in the Reynolds number resulting in a decrease in the peak combustion temperature. It was also found that the flameless combustion device has a critical Reynolds number, with flameless combustion only occurring when the Reynolds number was greater than 1.0×104. When the Reynolds number was lower than 1.0×104, the recirculation rate in the furnace was low, and the low *Kv* value meant that the recirculation rate in the furnace was very low, which was not enough to maintain sufficient dilution of the reactants in the flue gas, and the flameless combustion turns into flame combustion state.

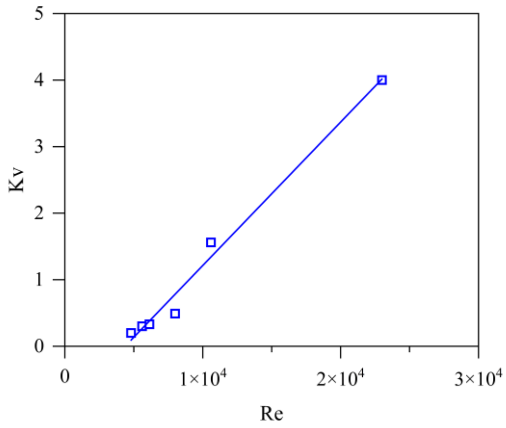

Fig. 13. Relationship between Reynolds number and recirculation rate at the nozzle

4.Conclusions

The effect of different inlet diameters and different inlet angles on achieving flameless combustion were investigated for the flameless combustion process under normal air conditions using methane as fuel under the conditions shown in tab. 1. The following main conclusions were drawn:

1.When combustion transitions from flamed to flameless combustion, temperature fluctuations become even, with temperature fluctuations of less than 15% in the furnace chamber and a significant reduction in the amount of NO_x.

2. With the increasing jet velocity, the area of OH radical and H_2CO radical are decreasing, which indicates that the high temperature and low temperature regions of the reaction are decreasing, and the temperature in the furnace gradually becomes average.

3. With the increase of burner inlet angle and inlet velocity, the area of OH radicals and H_2CO radicals decreases and gradually moves forward, and the flamed combustion state transitions to flameless combustion state.

4. With the increase of Reynolds number, the entrainment rate of flue gas increases, and the combustion state is closer to flameless combustion. When recirculation rate *Kv* >2, combustion becomes flameless.

5. The flameless combustion device had a critical Reynolds number, and flameless combustion could only occur when the Reynolds number was greater than 1.0×10^4.

Acknowledgment

We gratefully acknowledge the support from the Foundation of the State Key Laboratory of Natural Science Foundation of Neimenggu Province. We also thank all of the reviewers for providing insightful comments, the addressing of which has significantly strengthened our paper.

Corresponding Author

Jun Huang*, E-mail: hjun8420@imust.edu.cn

Author

Yazhu Zhang, E-mail: 13848236375@126.com
Congxi Liu, E-mail: L15731026768@163.com
Zhuben Huang, E-mail: 1585722613@qq.com
Li Zhang, E-mail: 804934133@qq.com
Kai Li, E-mail: 466806228@qq.com

Present Addresses

School of Energy and Environment, Inner Mongolia University of Science and Technology, Baotou 014010，People’s Republic of China.

Author Contributions

The manuscript was written through contributions of all authors. All authors have given approval to the final version of the manuscript. Yazhu Zhang: Writing - review and editing. Congxi Liu and Zhuben Huang: Writing original draft. Jun Huang: Visualization, Investigation. Li Zhang: Software, Data curation. Kai Li: Conceptualization.

Declaration of Competing Interest

The authors declare that they have no known competing financial interests or personal relationships that could have appeared to influence the work reported in this paper.

Funding Sources

Natural Science Foundation of Neimenggu Province(2019MS05012)
Natural Science Foundation of Neimenggu Province(2022MS05024)

REFERENCES

[1] Li P., *et al*., Experimental and Numerical Study of the Fuel-NO_x Formation at High CO_2 Concentrations in a Jet-Stirred Reactor, *Energy and Fuels*, 33 (2019), 7, pp. 6797-6808

[2] Slefarski, R., *et al*., Experimental study on combustion of CH_4/NH_3 fuel blends in an industrial furnace operated in flameless conditions, *Thermal Science*, 24 (2020). 2, pp. 3625-3635

[3] Pramanik S.,Ravikrishna RV., Effect of N_2 dilution and preheat temperature on combustion dynamics of syngas in a reverse-flow combustor, Experimental *Thermal and Fluid Science*, 110 (2020)

[4] Darvell., *et al*. Some Aspects of Modeling NO_x Formation Arising from the Combustion of 100% Wood in a Pulverized Fuel Furnace, *Combustion Science and Technology*, 186 (2014), 4-5, pp. 672-683

[5] Shan, Shiquan., *et al*., A review on fundmental research of oxy-coal combustion technology, *Thermal Science*, 26 (2022), 2, pp. 1945-1958

[6] Fan, WD., *et al*., Coal-nitrogen release and NO_x evolution in the oxidant staged combustion of coal, *Energy*, 125 (2017), pp. 417-426

[7] Tu Y,Zhou., *et al*., NO_x reduction in a 40 t/h biomass fired grate boiler using internal flue gas recirculation technology, *Applied Energy*, 220 (2018), pp. 962-973

[8] Christos A T., Emissions and Power Losses due to Biofuel or Biomass Nitrogen: Assessment and Prevention Mechanisms, *Energy Fuels*, 30 (2016), 11, pp. 9396-9408

[9] Cai, X., *et al*., New weighted-sum-of-gray-gases radiation model for oxy-fuel combustion simulation of semi-coke from coal-based poly-generation, *Thermal Science and Engineering Progress*, 46(2023)

[10] Wünning J.A., Wünning J.G.; Flameless oxidation to reduce thermal no-formation, *Progress in Energy and Combustion Science*, 23 (1997), 1, pp. 81-94

[11] Jianwei Y, Ichiro N 1999, Effects of Air Dilution on Highly Preheated Air Combustion in a Re-generative Furnace, *Energy and Fuels*, 13, pp. 99-104.

[12] G.G. Szegö., *et al*.,Operational characteristics of a parallel jet MILD combustion burner system, *Combustion and Flame*, 156 (2008), 2, pp. 429-438

[13] Masashi K., Toshiaki H., The science and technology of combustion in highly preheated air, *Symposium (International) on Combustion*, 27 (1998), 2, pp. 3135-3146

[14] Kazuhiro K., *et al*., High temperature air combustion boiler for low BTU gas, *Energy Conversion and Management*, 43(2002), 9-12, pp. 1563-1570.

[15] Liu W., *et al*., Effects of the tertiary air injection port on semi-coke flameless combustion with

coal self-preheating technology, *Fuel*, 271 (2020)

[16] Masashi K., Toshiaki H., The science and technology of combustion in highly preheated air, *Symposium (International) Combustion*, 27 (1998), 2, pp. 3135-3146

[17] Dally B.B., *et al.*, Structure of turbulent non-premixed jet flames in a diluted hot coflow, *Proceedings of Combustion Institute*, 29 (2002), 1, pp. 1147-1154

[18] F.C. Christo.,B.B. Dally., Modeling turbulent reacting jets issuing into a hot and diluted coflow. *Combustion and Flame*, 142 (2005), 1-2, pp. 117-129

[19] Seung H K., *et al*., Conditional moment closure modeling of turbulent nonpremixed combustion in diluted hot coflow, *Proceedings of the Combustion Institute,* 30 (2005), 1, pp. 751-757

[20] Dally B.,*et al*., Effect of fuel mixture on moderate and intense low oxygen dilution combustion, *Combustion and Flame*, 137 (2004), 4, pp. 418-431

[21] Roman W., *et al*., On the (MILD) combustion of gaseous, liquid, and solid fuels in high temperature preheated air, *Proceedings of the Combustion Institute*, 30 (2005), 2, pp. 2623-2629

[22] Veríssimo A.S., *et al*., Experimental study on the influence of the thermal input on the reaction zone under flameless oxidation conditions, *Fuel Processing Technology*, 106 (2013), pp. 423-428

[23] Huang MM., *et al*., Effect of thermal input, excess air coefficient and combustion mode on natural gas MILD combustion in industrial-scale furnace, *Fuel*, 302 (2021)

[24] Dally B.B., *et al*., Structure of turbulent non-premixed jet flames in a diluted hot coflow, *Proceedings of the Combustion Institute*, 29 (2002), 1, pp. 1147-1154

[25] Oldenhof E., *et al*., Ignition kernel formation and lift-off behaviour of jet-in-hot-coflow flames, *Combustion and Flame*, 157 (2010), 6, pp. 1167-1178

[26] Veríssimo A. S., *et al*., Operational, Combustion, and Emission Characteristics of a Small-Scale Combustor, *Energy Fuels*, 25 (2011), 6, pp. 2469-2480

[27] Von Schéele, J., *et al.*, Flameless oxyfuel combustion for increased production and reduced CO2 and NOx emissions, *stahl und eisen,* 128 (2008), 7, pp. 35-42

[28] Szewczyk, D., *et al*., Experimental study of the combustion process of gaseous fuels containing nitrogen compounds with the use of new, low-emission Zonal Volumetric Combustion technology, *Energy*, 92 (2015), pp. 3-12

[29] Mardani A, *et al*., Numerical study of oxy-fuel MILD (moderate or intense low-oxygen dilution combustion) combustion for CH_4-H_2 fuel, *Energy*, 99 (2016), pp. 136 -151

[30] Dostiyarov, A., *et al*., A novel vortex combustion device: Experiments and numerical simulations with emphasis on the combustion process and NO_x emissions, *Thermal Science*, 26 (2022), 2, pp.1971-1983

Submitted: 14.10.2023.
Revised: 31.01.2024.
Accepted: 12.02.2024.